

$$\begin{aligned}
\Delta_0(i) &= M_0(B_i(x), A_i(y)) - M_0(A_i(x) - 1, A_i(y)) \\
\Delta_1(i) &= M_1(B_i(x), A_i(y) - A_i(x)) - M_1(A_i(x) - 1, A_i(y) - A_i(x)) \\
\Delta_2(i) &= M_2(A_i(x), B_i(y)) - M_2(A_i(x), A_i(y) - 1) \\
\Delta_3(i) &= M_3(A_i(x) + A_i(y), B_i(y)) - M_2(A_i(x) + A_i(y), A_i(y) - 1)
\end{aligned} \tag{14}$$

of  $\sum_G g^2(x, y)$  can be speeded up by a preprocessing like that for (13). We have decided not to lengthen this correspondence by the tedious derivation of this time-saving technique. We instead simply state our result that  $\sum_G g^2(x, y)$  can be evaluated in  $O(1)$  time for any given  $G$  with an  $O(|\mathcal{G}|)$  preprocessing and  $O(|\mathcal{G}|)$  space.

Since an optimal bipartition of  $G$  can be done in  $O(\sum_{0 \leq j \leq 3} L_j)$  time, the worst-case time complexity of the ROFS algorithm aided by the preprocessing can be bounded by  $O(K(N_x + N_y))$ . If we assume that, on average, each bipartition of  $G$  halves  $G$  in size and each cutting direction has equal chance to the optimal one (and denote by  $C(n)$  the cost of bipartitioning a subimage of size  $n$ ), then the total cost of the procedure ROFS becomes  $\sum_{i=0}^{\log K} 2^i C(|\mathcal{G}|/2^i)$ . Under the above assumptions, we have  $C(n) = O(n^{0.5})$  since  $G$  is not extremely prolonged in any cutting direction. Thus, the expected time complexity of the ROFS algorithm is  $\sum_{i=0}^{\log K} 2^i C(|\mathcal{G}|/2^i) = O((K|\mathcal{G}|)^{0.5})$ .

The required preprocessing of computing (13) clearly takes  $O(|\mathcal{G}|)$  operations and  $O(|\mathcal{G}|)$  space, based on the parameter ranges in (13). Thus, the cost of the preprocessing asymptotically dominates that of the ROFS algorithm in the expected case for  $K \ll |\mathcal{G}|$ . However, this will only be true for very large  $|\mathcal{G}|$  because there is a considerable constant before the order complexity  $O((K|\mathcal{G}|)^{0.5})$  incurred by the overheads of computing the key vertices of newly formed canonical polygons and polygon scan conversion to determine the digital cutting line segment  $A_i B_i$ .

## VI. CONCLUSION

The recursive optimal four-way split and the RAG-guided minimum cost merge were proposed to improve the validity of the classic split-and-merge segmentation algorithm. The new optimized split-and-merge algorithm achieves the unification of edge detection and segmentation within a tree hierarchy. As a result of this data structure and a statistic preprocessing, the optimization can be done without increasing the time complexity order of the previous algorithms.

The success of the adaptive four-way split naturally leads to the following question: Why should we not consider every orientation when we optimize the split to capture edges of arbitrary orientations? This is a matter of compromise between computational costs and the optimality. Although adaptive four-way cuts greatly improve the segmentation validity over regular rectilinear cuts, they still have relatively simple digital geometry and manageable computational cost. The same cannot be said when, say, eight different cutting directions are considered in the optimization.

## REFERENCES

- [1] D. Ballard and C. M. Brown, *Computer Vision*. Englewood Cliffs, NJ: Prentice-Hall, 1982.

- [2] J. D. Foley, A. V. Dam, S. K. Feiner, and J. F. Hughes, *Computer Graphics, Principles and Practice*. Reading, MA: Addison-Wesley, 1990, 2nd ed.
- [3] D. E. McClure, "Nonlinear segmented function approximation and analysis of line patterns," *Quar. Applied Math.*, vol. 33, pp. 1-37, 1975.
- [4] T. Pavlidis, *Structural Pattern Recognition*. New York: Springer, 1977.
- [5] —, *Algorithms for Graphics and Image Processing*. Rockville, MD: Computer Science, 1982.
- [6] H. Samet, "The quadtree and related hierarchical data structures," *Comput. Surveys*, vol. 16, no. 2, pp. 187-230, June 1984.
- [7] X. Wu, "Image coding by adaptive tree-structured segmentation," *IEEE Trans. Inform. Theory*, vol. 38, no. 6, pp. 1755-1767, Nov. 1992.

## Shape from Shading with a Linear Triangular Element Surface Model

Kyong Mu Lee and C.-C. Jay Kuo

**Abstract**—We propose to combine a triangular element surface model with a linearized reflectance map to formulate the shape-from-shading problem. The main idea is to approximate a smooth surface by the union of triangular surface patches called triangular elements and express the approximating surface as a linear combination of a set of nodal basis functions. Since the surface normal of a triangular element is uniquely determined by heights of its three vertices (or nodes), image brightness can be directly related to nodal heights via the linearized reflectance map. The surface height can then be determined by minimizing a quadratic cost functional corresponding to the squares of brightness errors and solved effectively with the multigrid computational technique. The proposed method does not require any integrability constraint or artificial assumptions on boundary conditions. Simulation results for synthetic and real images are demonstrated to show the performance and efficiency of our new method.

**Index Terms**—Computer vision, shape from shading, surface model, triangular element.

## I. INTRODUCTION

The shape-from-shading (SFS) problem extracts 3-D shape information from one or multiple 2-D shading images and can be viewed as an inversion problem of image formation. It was first formulated

Manuscript received March 1, 1991; revised March 2, 1992. This work was supported by the USC Faculty Research and Innovation Fund and a National Science Foundation Research Initiation Award (ASC-9009323). Recommended for acceptance by Associate Editor Y. Aloimonos.

The authors are with the Signal and Image Processing Institute and the Department of Electrical Engineering-Systems, University of Southern California, Los Angeles, California 90089-2564.

IEEE Log Number 9208438.

by Horn [6], [7] and has been studied intensively for the last two decades [2], [4], [5], [9]–[12], [16], [17], [20], [21], [24], [25], [30], [31].

Most research work on SFS with a single image uses the variational approach [4], [9], [10], [12], [17], [24] in which a surface orientation field characterized by its slopes  $p(x, y) = \partial z(x, y)/\partial x$  and  $q(x, y) = \partial z(x, y)/\partial y$  is determined by minimizing a cost functional of brightness errors. To achieve the objective, one applies the calculus of variations [3] to the functional to derive a set of coupled Euler equations involving  $p(x, y)$  and  $q(x, y)$ . However, a straightforward implementation of this approach does not work properly due to the nonintegrability of computed  $p(x, y)$  and  $q(x, y)$  and the ill-posed nature of the problem. Methods for enforcing integrability have been studied by Frankot and Chellappa [4] and Horn [9]. The ill-posedness of SFS is often handled by regularization [1], [12], [22].

Since the variational approach leads to complicated first-order nonlinear partial differential equations (PDE's), modified SFS algorithms still have two major difficulties. First, appropriate boundary conditions are needed for PDE solution. No boundary conditions result in the ambiguity of the solution and the instability of the numerical algorithm [9]. Second, nonlinear PDE's are solved by iterative algorithms whose convergence property is, however, not yet well understood [9], [10], [17]. The number of iterations of converging algorithms often grows linearly with image size  $N$  [9] so that computational complexity is proportional to  $O(N^2)$ , which is too high to be useful in real-time applications.

A very different approach for SFS was recently proposed by Pentland [21]. It relates image brightness to surface height  $z(x, y)$  in closed form with a linearized reflectance map in the Fourier transform domain. The resulting algorithm is a nonoptimization and noniterative one. Since surface height  $z(x, y)$ , rather than its slopes  $p(x, y)$  and  $q(x, y)$ , is computed directly from the algorithm, no integrability problem appears. However, the reconstructed surface by this approach is less accurate than that obtained by the variational approach since it is a one-step algorithm using only the global linearization of the reflectance map around the origin. Other shortcomings of the approach include that known physical information cannot be easily incorporated in the formulation and that it is sensitive to the noise.

We propose a new approach to SFS in this research. The basic idea of our approach is to approximate a smooth surface by the union of triangular surface patches called *triangular elements* and express the approximating surface as a linear combination of a set of nodal basis functions of compact support. Since the surface normal of a triangular element is linearly determined by heights of its three vertices (or nodes), we can relate image brightness directly to nodal heights via the reflectance map. Furthermore, image brightness is an affine function of nodal heights if the reflectance map is linearized. By defining the cost functional to be the squares of brightness errors, we are led to a quadratic functional minimization problem parameterized by nodal heights. Our approach has several unique features. First, it does not need any integrability constraint since the height is computed directly. Second, boundary conditions are not needed in the solution process since it solves a discrete minimization problem rather than discretized PDE's. Third, since the cost functional is greatly simplified to be a quadratic form, it is much easier to analyze the existence and uniqueness of the solution and to search effective convergent iterative algorithms. Besides, the optimization problem can be transformed into the solution of a large sparse linear system of equations, and very efficient multigrid (MG) computational algorithm can be conveniently applied. The number of iterations for the MG algorithm is independent of image size  $N$  so that its computational complexity is only  $O(N)$ .

To use height values directly as variables in SFS has been con-

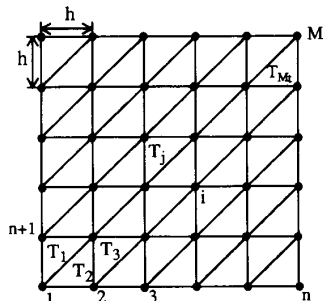


Fig. 1. Uniform triangulation of a square domain  $\Omega$ .

sidered by several researchers. In [9], Horn used both the height and gradients as variables so that the height was recovered directly without integration. However, boundary conditions were still needed for PDE solution in his work. It is also worthwhile to point out a very recent work by Leclerc and Bobick [15], which recovered heights directly using a discrete minimization formulation. Their idea is similar to ours except that they did not use an explicit surface model. Instead, the horizontal and vertical central differences of the height  $z(x, y)$  were used to approximate the gradients  $p$  and  $q$ . Besides, no linearization of the reflectance map was made, and the corresponding nonlinear cost functional was solved by the conjugate gradient method.

## II. SHAPE-FROM-SHADING PROBLEM FORMULATION

### A. Triangular Element Surface Model

A smooth surface can be approximated by a union of triangular surface patches and expressed as a linear combination of nodal basis functions with compact support known as the finite triangular elements [13], [23]. For convenience, some notation is introduced as follows. A uniform triangulation of a square domain  $\Omega$  with spacing  $h$  is illustrated in Fig. 1, where the domain  $\Omega$  is divided into a set of nonoverlapping triangles  $T_i$

$$\Omega = \bigcup_{1 \leq i \leq M_t} T_i, \quad (2.1)$$

and where  $M_t$  is the number of triangles. Let  $V_h$  denote the set of continuous piecewise linear surfaces defined on  $\Omega$  and linear over all triangles  $T_i$ . The nodal basis function  $\phi_i \in V_h$  is the function that takes unity at the  $i$ th node and zero at other nodes (see Fig. 2). It is easy to see that any  $z \in V_h$  can be represented as the linear combination of nodal basis functions

$$z(x, y) = \sum_{i=1}^{M_n} z_i \phi_i(x, y), \quad (2.2)$$

where  $z_i$  is the value of  $z(x, y)$  at the  $i$ th node, and  $M_n$  is the number of nodal basis functions.

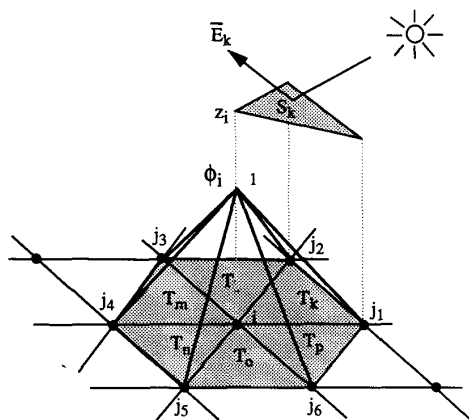
The gradient  $(p, q)$  of the surface  $z(x, y)$  can be computed as

$$p(x, y) = \frac{\partial z(x, y)}{\partial x} = \sum_{i=1}^{M_n} z_i \frac{\partial \phi_i(x, y)}{\partial x}, \quad (2.3)$$

and

$$q(x, y) = \frac{\partial z(x, y)}{\partial y} = \sum_{i=1}^{M_n} z_i \frac{\partial \phi_i(x, y)}{\partial y}. \quad (2.4)$$

Since the partial derivatives of  $\phi_i(x, y)$  with respect to  $x$  and  $y$  are simply some constants so that  $p(x, y)$  and  $q(x, y)$  are linear


 Fig. 2. Nodal basis function  $\phi_i$ .

functions of nodal heights  $z_i$ . Note also that  $p(x, y)$  and  $q(x, y)$  are piecewise constant functions on  $\Omega$ , and they take constant values on each triangular domain  $T_i$ .

### B. Reflectance Map Image Formation Model

Under the assumption of the orthographic projection, the Lambertian surface, and a distant single point light source, the irradiance or brightness  $E$  at a given point  $(x, y)$  is primarily due to the surface orientation at that point. This relationship is described by the *image irradiance equation* [8], [11]

$$E(x, y) = R(p, q) \quad (2.5)$$

where  $R$  is called the reflectance map function. The form of  $R$  is usually chosen as

$$R(p, q) = \begin{cases} \eta \frac{1+p_s p + q_s q}{\sqrt{(1+p^2+q^2)}\sqrt{(1+p_s^2+q_s^2)}}, & 1+p_s p + q_s q \geq 0, \\ 0, & 1+p_s p + q_s q < 0 \end{cases} \quad (2.6a)$$

or equivalently

$$R(p, q) = \begin{cases} \eta \frac{K}{\sqrt{(1+p^2+q^2)}}, & K \geq 0, \\ 0, & K < 0. \end{cases} \quad (2.6b)$$

$$K = -p \cos \tau \sin \sigma - q \sin \tau \sin \sigma + \cos \sigma$$

where  $\eta$  is the albedo of the surface,  $(p, q)$  the gradient of the surface at point  $(x, y)$ ,  $(-p_s, -q_s, 1)$  the illumination direction pointing toward the light source, and  $\tau$  and  $\sigma$  the *tilt* and *slant* angles that the illumination direction makes with the  $x$  and  $z$  axes, respectively.

As given in (2.6), the reflectance map  $R$  is a nonlinear function that can be depicted as nested contours in the gradient space  $(p, q)$ . To remove the nonlinearity, techniques based on the linear approximation of the reflectance map have been recently proposed [9], [21], that is, we take the Taylor series expansion of  $R(p, q)$  about a certain reference point  $(p_0, q_0)$  through the first-order term

$$R(p, q) \approx R(p_0, q_0) + (p - p_0) \frac{\partial R(p, q)}{\partial p} \Big|_{(p_0, q_0)} + (q - q_0) \frac{\partial R(p, q)}{\partial q} \Big|_{(p_0, q_0)}. \quad (2.7)$$

The reference point  $(p_0, q_0)$  can be either fixed or varying for different values of  $(p, q)$ .

### C. Image Formation on Modeled Surfaces

By substituting (2.3) and (2.4) into (2.7), we have

$$R(p, q) \approx \alpha p + \beta q + \gamma = \sum_{i=1}^{M_n} \Phi_i z_i + \gamma \quad (2.8)$$

where

$$\Phi_i(x, y) = \alpha \frac{\partial \phi_i(x, y)}{\partial x} + \beta \frac{\partial \phi_i(x, y)}{\partial y}, \quad (2.8a)$$

$$\gamma = R(p_0, q_0) - \alpha p_0 - \beta q_0$$

and where

$$\alpha = \frac{\partial R(p, q)}{\partial p} \Big|_{(p_0, q_0)}, \quad \beta = \frac{\partial R(p, q)}{\partial q} \Big|_{(p_0, q_0)}. \quad (2.8b)$$

Thus, combining (2.5) and (2.8), one can establish a linear relationship between the image brightness  $E(x, y)$  and nodal values  $z_i$ ,  $1 \leq i \leq M_n$

$$E = \alpha p + \beta q + \gamma = \sum_{i=1}^{M_n} \Phi_i z_i + \gamma. \quad (2.9)$$

To estimate the nodal heights  $z_i$  based on the shading information, we consider the cost functional

$$\mathcal{E}_b = \int \int_{\Omega} (E_o - E_r)^2 dx dy \quad (2.10)$$

where  $E_o$  is the observed image intensity,  $E_r$  is the image intensity formed by the reconstructed surface via (2.9), and the subscript  $b$  denotes the cost due to the brightness error. By substituting (2.9) into (2.10), we obtain

$$\mathcal{E}_b = \int \int_{\Omega} [E_o - (\sum_{i=1}^{M_n} \Phi_i z_i + \gamma)]^2 dx dy = \frac{1}{2} \mathbf{z}^T \mathbf{A} \mathbf{z} - \mathbf{b}^T \mathbf{z} + c \quad (2.11)$$

where  $\mathbf{z}$  is the vector of nodal variables, and the elements  $a_{i,j}$  and  $b_i$  of matrix  $\mathbf{A}$  and vector  $\mathbf{b}$  can be determined, respectively, as

$$a_{i,j} = 2 \int \int_{\Omega} \Phi_i \Phi_j dx dy, \quad (2.12)$$

$$b_i = 2 \int \int_{\Omega} (E_o - \gamma) \Phi_i dx dy \quad 1 \leq i, j \leq M_n.$$

Following the finite-element terminology,  $\mathbf{A}$  is called the *stiffness* matrix, and  $\mathbf{b}$  the *load* vector. Our objective is to determine the nodal height vector  $\mathbf{z}$  that minimizes the quadratic functional (2.11). Note that the minimization problem can also be formulated as the solution of a system of linear equations

$$\mathbf{A} \mathbf{z} = \mathbf{b}. \quad (2.13)$$

It is obvious that the quadratic functional gives a unique minimum only when the *stiffness* matrix  $\mathbf{A}$  is positive definite. The property of  $\mathbf{A}$  will be discussed in Section IV.

### III. CONSTRUCTION OF STIFFNESS MATRICES AND LOAD VECTORS

Note that  $a_{i,j} = 0$  if  $i$  and  $j$  are not the neighboring nodal points since either  $\Phi_i(x, y)$  or  $\Phi_j(x, y)$  is zero for  $(x, y) \in \Omega$ . Thus, we only have to determine that  $a_{i,j}$  is equal to either the node  $i$  or one of its six neighboring nodes  $j_1, \dots, j_6$  as shown in Fig. 2. We use  $T_k, \dots, T_p$  to denote the six triangular domains surrounding node  $i$ , and  $S_k, \dots, S_p$  the triangular surface patches defined on  $T_k, \dots, T_p$ .

TABLE I  
ELEMENTS OF STIFFNESS MATRIX  $\mathbf{A}$

$a_{i,i}$	$\alpha_k^2 + \beta_l^2 + (\alpha_m - \beta_m)^2 + \alpha_n^2 + \beta_o^2 + (\alpha_p - \beta_p)^2$
$a_{i,j_1}$	$\alpha_k(\beta_k - \alpha_k) + \alpha_p(\beta_p - \alpha_p)$
$a_{i,j_2}$	$-(\alpha_k\beta_k + \alpha_l\beta_l)$
$a_{i,j_3}$	$\beta_l(\alpha_l - \beta_l) + \beta_m(\alpha_m - \beta_m)$
$a_{i,j_4}$	$\alpha_m(\beta_m - \alpha_m) + \alpha_n(\beta_n - \alpha_n)$
$a_{i,j_5}$	$-(\alpha_n\beta_n + \alpha_o\beta_o)$
$a_{i,j_6}$	$\beta_o(\alpha_o - \beta_o) + \beta_p(\alpha_p - \beta_p)$

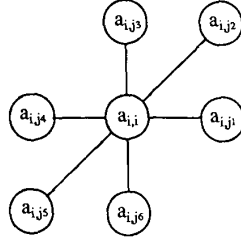


Fig. 3. Seven-point stencil nodal operator.

One can determine the gradients of the nodal basis function  $\phi_i(x, y)$  on triangles  $T_k, \dots, T_p$  from Fig. 2. They are

$$\left( \frac{\partial \phi_i(x, y)}{\partial x}, \frac{\partial \phi_i(x, y)}{\partial y} \right) = \begin{cases} (-h^{-1}, 0), & \text{for } (x, y) \in T_k, \\ (0, -h^{-1}), & \text{for } (x, y) \in T_l, \\ (h^{-1}, -h^{-1}), & \text{for } (x, y) \in T_m, \\ (h^{-1}, 0), & \text{for } (x, y) \in T_n, \\ (0, h^{-1}), & \text{for } (x, y) \in T_o, \\ (-h^{-1}, h^{-1}), & \text{for } (x, y) \in T_p. \end{cases} \quad (3.1)$$

where  $h$  is the spacing.

Consider the linearization of the reflectance map (2.8) by using different reference gradients for different triangles. Let  $(p_{0i}, q_{0i})$  be the reference gradient and  $\alpha_i, \beta_i$ , and  $\gamma_i$  be the coefficients of the linearized reflectance map on triangular domain  $T_i$ . By using (2.12), we can express the elements of  $\mathbf{A}$  and  $\mathbf{b}$  in terms of  $\alpha_i, \beta_i$ , and  $\gamma_i$  in a straightforward way.

The diagonal element  $a_{i,i}$  of  $\mathbf{A}$  can be determined [18] as

$$a_{i,i} = \alpha_k^2 + \beta_l^2 + (\alpha_m - \beta_m)^2 + \alpha_n^2 + \beta_o^2 + (\alpha_p - \beta_p)^2$$

where  $\alpha_k, \dots, \alpha_p$  and  $\beta_k, \dots, \beta_p$  are coefficients of linearized reflectance maps on triangles  $T_k, \dots, T_p$ . The off-diagonal element of  $\mathbf{A}$  also can be derived similarly, and the results are summarized in Table I.

We can represent the corresponding nodal operator by a seven-point stencil as illustrated in Fig. 3. Finally, the element  $b_i$  of the load vector  $\mathbf{b}$  can be obtained [18] by

$$b_i = h[-\alpha_k(\bar{E}_k - \gamma_k) - \beta_l(\bar{E}_l - \gamma_l) + (\alpha_m - \beta_m)(\bar{E}_m - \gamma_m) + \alpha_n(\bar{E}_n - \gamma_n) + \beta_o(\bar{E}_o - \gamma_o) + (\beta_p - \alpha_p)(\bar{E}_p - \gamma_p)] \quad (3.2)$$

where  $\bar{E}_k, \dots, \bar{E}_p$  denote the average brightness on the triangles  $T_k, \dots, T_p$ .

One special case of the linearization scheme is to choose the reference  $(p_0, q_0)$  to be the same for all triangular surface patches. We call it the *global linearization* and denote the corresponding stiffness matrix by  $\mathbf{A}_g$ . The elements  $a_{i,j}$  of  $\mathbf{A}_g$  can be further simplified and

TABLE II  
COEFFICIENTS OF GLOBAL STIFFNESS MATRIX  $\mathbf{A}_g$

$a_{i,i}$	$2(\alpha^2 - \alpha\beta + \beta^2)$
$a_{i,j_1}, a_{i,j_4}$	$2\alpha(\beta - \alpha)$
$a_{i,j_2}, a_{i,j_5}$	$-2\alpha\beta$
$a_{i,j_3}, a_{i,j_6}$	$2\beta(\alpha - \beta)$

summarized in Table II. Since the values of  $\alpha, \beta$ , and  $\gamma$  are the same for all triangular domains, their subscripts are dropped.

Suppose that we do not have any *a priori* knowledge of the reconstructed surface; we may set all initial nodal values zero and proceed as follows.

#### Algorithm I: The Basic SFS Algorithm

##### Initialization ( $k = 0$ )

Set the reference gradient  $(p_{0i}^0, q_{0i}^0)$  at every triangle  $T_i$  to be  $(0, 0)$ , and construct the global stiffness matrix  $\mathbf{A}_g^0$  and the load vector  $\mathbf{b}^0$ . Solve  $\mathbf{A}_g^0 \mathbf{z}^0 = \mathbf{b}^0$  for nodal values  $\mathbf{z}^0$ .

##### Iterations ( $k = 1, 2, \dots$ )

Set the reference gradient  $(p_{0i}^k, q_{0i}^k)$  at triangle  $T_i$  to be the local gradient determined by nodal values  $\mathbf{z}^{k-1}$  and construct the corresponding stiffness matrix  $\mathbf{A}_l^k$  and load vector  $\mathbf{b}^k$ , where the subscript  $l$  denotes local linearization. Solve  $\mathbf{A}_l^k \mathbf{z}^k = \mathbf{b}^k$  for nodal values  $\mathbf{z}^k$ .

If  $\|\mathbf{z}^k - \mathbf{z}^{k-1}\| < \epsilon$ , where  $\epsilon$  is a predefined small quantity, then  $\mathbf{z}^k$  is the desired solution. Otherwise, go to the next iteration.

In the above algorithm, we use a *successive linearization* scheme, where the linearization of the reflectance map is performed based on the local gradients obtained from the previous iteration. The motivation is simple. There are two kinds of error introduced in our SFS formulation: the surface approximation error introduced by the triangular element model and the reflectance map approximation error due to linearization. The first kind of error depends on the spacing  $h$  and can be reduced by using smaller spacings. The second kind of error can be reduced by approximating the reflectance map to the original nonlinear one as close as possible. Since the coefficients  $\alpha_i$  and  $\beta_i$  are functions of local reference gradients  $(p_{0i}, q_{0i})$ , the choice of  $(p_{0i}, q_{0i})$  is important. To determine appropriate local reference gradients, we need good surface information. By doing the successive linearization, we can get increasingly accurate surface gradients and surface values.

#### IV. SINGULARITIES OF STIFFNESS MATRICES

The stiffness matrix  $\mathbf{A}$  is *sparse* since each nodal basis function  $\phi_i(x, y)$  has a compact support and overlaps with only a finite number ( $\leq 6$ ) of neighboring nodal basis functions. It is evident from (2.12) that  $a_{i,j} = a_{j,i}$  so that  $\mathbf{A}$  is *symmetric*. Besides, for any nonzero vector  $\mathbf{z}$ , we have

$$\mathbf{z}^T \mathbf{A} \mathbf{z} = \sum_{i=1}^{M_n} \sum_{j=1}^{M_n} z_i a_{i,j} z_j = 2 \int \int_{\Omega} \left[ \sum_{i=1}^{M_n} \Phi_i z_i \right]^2 dx dy \geq 0 \quad (4.1)$$

so that  $\mathbf{A}$  is *positive semidefinite*. However,  $\mathbf{A}$  is singular, and consequently, the cost functional given in (2.11) does not have a unique minimum. In this section, we will investigate the reasons (or physical interpretations) for the singularity of  $\mathbf{A}$  and discuss ways to remove it.

### A. Stiffness Matrix with Global Linearization

One reason for  $\mathbf{A}_g$  to be singular can be explained by the well-known fact that we cannot determine the absolute heights of the object surface from the image plane since the brightness of a surface patch is only determined by its gradient. According to Table II, it is easy to verify that the row sum of  $\mathbf{A}_g$  is zero for every row. Let  $\mathbf{u}$  be the vector of 1's, i.e.,  $\mathbf{u} = [1, 1, \dots, 1]^T$ . We have  $\mathbf{A}_g \mathbf{u} = \mathbf{0}$ . Therefore, if  $\mathbf{A}_g \mathbf{z}^* = \mathbf{b}$

$$\mathbf{A}_g(\mathbf{z}^* + c\mathbf{u}) = \mathbf{b} \quad (4.2)$$

where  $c$  is an arbitrary constant. This singularity is clearly the inherent limitation of the SFS problem. However, it can be removed by introducing an arbitrary reference nodal point.

Another reason for  $\mathbf{A}_g$  to be singular can be understood by considering a single triangular patch. Suppose that one node is chosen to be the reference. There are still two nodal heights to be determined. Since the image irradiance equation  $R(p, q) = E$ , where  $E$  is the average brightness on the patch, only provides one constraint, the two equations consisting of these two relative nodal heights have to be linearly dependent. Hence, we conclude that the global stiffness matrix  $\mathbf{A}_g$  has a null space of dimension of at least two.

The singularity of  $\mathbf{A}_g$  may also be resulted from special values of  $\alpha$  and  $\beta$ , that is, if  $\alpha = 0$ ,  $\beta = 0$ , or  $\alpha = \beta$ , we are not able to relate the gradient of a surface patch to its image intensity via (2.9). To see this, let us consider the triangular surfaces  $S_k, \dots, S_p$  over the triangular domains  $T_k, \dots, T_p$  as specified in Fig. 2. If  $\alpha = 0$  (or  $\beta = 0$ ), the image intensities of surfaces  $S_k$  and  $S_n$  (or  $S_l$  and  $S_o$ ) are independent of  $p$  (or  $q$ ) and, thus, the nodal height  $z_i$ . This phenomenon can also be explained by using Table II. Note that

$$\begin{aligned} a_{i,j_1} = a_{i,j_4} = a_{i,j_2} = a_{i,j_5} = 0, & \quad \text{if } \alpha = 0. \\ a_{i,j_3} = a_{i,j_6} = a_{i,j_2} = a_{i,j_5} = 0, & \quad \text{if } \beta = 0. \end{aligned}$$

Similarly, we have

$$a_{i,j_1} = a_{i,j_4} = a_{i,j_3} = a_{i,j_6} = 0, \quad \text{if } \alpha = \beta.$$

It follows that if  $\alpha = \beta$ , the image intensities of surfaces  $S_m$  and  $S_p$  cannot be used to determine the nodal height  $z_i$ .

Motivated by the previous discussion, the sufficient conditions for the quadratic cost functional (2.11) to have a unique minimum can be stated as follows.

**Theorem 1:** The quadratic functional (2.11) with  $\mathbf{A} = \mathbf{A}_g$  has a unique minimum if the following two conditions are satisfied.

1. There are two neighboring nodal points whose heights are given.
2.  $\alpha \neq 0$ ,  $\beta \neq 0$ , and  $\alpha \neq \beta$ .

*Proof:* Without loss of generality, it is assumed that we know the two nodal heights of the triangular surface  $S_1$  over the domain  $T_1$ , as depicted in Fig. 4. If  $z_1$  and  $z_4$  are given since  $\alpha \neq 0$ , we can use the linearized reflectance map and the image irradiance equation to determine the value of  $z_5$ . Similarly, we can argue that  $z_1$  (or  $z_4$ ) can be obtained from given  $z_4$  and  $z_5$  (or  $z_1$  and  $z_5$ ). In turn, the nodal heights of adjacent triangular surface patches  $S_2, S_6$  can be determined since they share two common nodes with  $S_1$ . Thus, by this manner, all nodal values  $z_i$  can be uniquely determined.  $\square$

In practice, to achieve the first condition, we may simply select two neighboring nodal points in an estimated plane region as the zero reference points. Since  $\alpha$  and  $\beta$  are functions of the reference gradient  $(p_0, q_0)$ , the second condition can be satisfied by choosing a proper value of  $(p_0, q_0)$ . To give an example, consider the reflectance map (2.6) with the illumination direction  $(p_s, q_s, 1)$  and  $(p_0, q_0) = (0, 0)$ . It is straightforward to see that the second condition is satisfied except  $p_s = 0$ ,  $q_s = 0$ , or  $p_s = q_s$ . If the illumination direction happens to

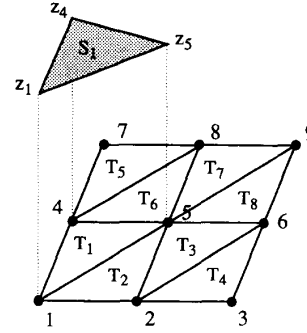


Fig. 4. Simple example of a triangularized domain.

be these cases, we may move the reference gradient slightly around the origin so that the second condition is still satisfied.

### B. Stiffness Matrix with Local Linearization

For general stiffness matrix  $\mathbf{A}$ , we can also state the sufficient conditions for the quadratic cost functional (2.11) to have a unique minimum as follows.

**Theorem 2:** The quadratic functional (2.11) has a unique minimum if the following two conditions are satisfied.

1. There are two neighboring nodal points whose heights are given.
2.  $\alpha_i \neq 0$ ,  $\beta_i \neq 0$  and  $\alpha_i \neq \beta_i$  for the linearized reflectance map defined on every domain  $T_i$ .

Its proof is omitted since it is very similar to that of Theorem 1. Note that these conditions are not necessary but are sufficient. For example, (2.11) may have a unique minimum even if the second condition is not satisfied. As before, the first condition can be satisfied by selecting two neighboring nodes in an estimated plane region as the zero reference points. To attain the second condition, one possibility is to consider the selection of a proper reference gradient for each triangle patch. This can be achieved by checking the values of  $\alpha_i, \beta_i$  and perturbing the reference point slightly whenever it is necessary. Another possibility is to introduce a regularization method to ensure the well posedness of the SFS problem.

### V. REGULARIZATION WITH SMOOTH SURFACE CONSTRAINT

Regularization is often achieved by adding some terms to the cost functional so that the regularized problem is well posed [1], [22], [29]. It is preferable that we associate the additional term with some physical interpretation. As discussed in Section IV, the nonuniqueness of the minimum of the quadratic functional (2.11) is primarily due to some free nodal variables that may have arbitrary values without affecting the cost functional. Therefore, to obtain a unique solution, we have to restrict these free variables by some constraint, say, the smoothness surface constraint, so that each node is related to its neighboring nodes through other means. Another reason to impose the smoothness constraint is to make our algorithm less sensitive to noises such as the sensor noise, the quantization noise, and the imperfect reflectance map model for real images.

To impose the smooth surface constraint, we define a new cost functional

$$\mathcal{E} = \mathcal{E}_b + \lambda \mathcal{E}_s \quad (5.1)$$

where  $\mathcal{E}_b$  is the original cost functional given by (2.11), and  $\lambda$  is the smoothing factor. The smoothing cost functional  $\mathcal{E}_s$  can be chosen

as a discrete version of *thin plate* energy model

$$\mathcal{E}_{s,c} = \frac{1}{2} \iint (z_{xx}^2 + 2z_{xy}^2 + z_{yy}^2) dx dy. \quad (5.2)$$

By discretizing (5.2), we obtain

$$\begin{aligned} \mathcal{E}_s = \frac{1}{2h^2} \sum_{n_x} \sum_{n_y} & [(z_{n_x+1, n_y} - 2z_{n_x, n_y} + z_{n_x-1, n_y})^2 \\ & + 2(z_{n_x+1, n_y+1} - z_{n_x, n_y+1} - z_{n_x+1, n_y} + z_{n_x, n_y})^2 \\ & + (z_{n_x, n_y+1} - 2z_{n_x, n_y} + z_{n_x, n_y-1})^2] \end{aligned}$$

where  $h$  is the spacing. We can also express (5.2) in matrix form as

$$\mathcal{E}_s = \frac{1}{2} \mathbf{z}^T \mathbf{B} \mathbf{z} \quad (5.3)$$

where  $\mathbf{z}$  is the vector of nodal variables, and  $\mathbf{B}$  is the *smoothness* matrix, which is sparse and symmetric. It is convenient to view the matrix-vector product  $\mathbf{B}\mathbf{z}$  as a local nodal operator operating on a 2-D array. The local nodal operator is of the following stencil form

$$\mathbf{B} : \frac{1}{h^2} \begin{vmatrix} & & 1 & & \\ & 2 & -8 & 2 & \\ 1 & -8 & 20 & -8 & 1 \\ & 2 & -8 & 2 & \\ & & 1 & & \end{vmatrix} \quad (5.4)$$

where  $h$  denotes the spacing between nodal points. Some special-operator stencils for nodal points near the boundary are given in [27] and [28].

Substituting (5.3) and (2.11) into (5.1), we obtain

$$\mathcal{E} = \frac{1}{2} \mathbf{z}^T \mathbf{C} \mathbf{z} - \mathbf{b}^T \mathbf{z} + c. \quad (5.5)$$

where

$$\mathbf{C} = \mathbf{A} + \lambda \mathbf{B}.$$

The following theorem states the conditions for the existence and uniqueness of the minimum of (5.5).

**Theorem 3:** The quadratic functional (5.5) has a unique minimum if the following two conditions are satisfied:

1. There is one nodal point whose height is given.
2. There exist at least one pair of coefficients  $(\alpha_i, \beta_i)$  and  $(\alpha_j, \beta_j)$  of the linearized reflectance maps over triangular domains  $T_i$  and  $T_j$  satisfying

$$\frac{\beta_i}{\alpha_i} \neq \frac{\beta_j}{\alpha_j}.$$

*Proof:* Since matrices  $\mathbf{A}$  and  $\mathbf{B}$  are both positive semidefinite,  $\mathbf{C} = \mathbf{A} + \lambda \mathbf{B}$  with  $\lambda > 0$  is also positive semidefinite. Thus, the minimum of the quadratic functional (5.5) exists. In the following, we want to show that under condition 2, the positive semidefinite matrix  $\mathbf{C}$  has only one eigenvalue equal to 0, which is associated with the eigenvector  $(1, 1, \dots, 1)$ . As a consequence, if both conditions 1 and 2 are met, the minimum is unique.

It is sufficient to prove that  $\mathbf{z}^T \mathbf{C} \mathbf{z} = 0$  only if  $\mathbf{z}$  is a constant vector. Let us rewrite  $\mathbf{z}^T \mathbf{C} \mathbf{z}$  as

$$\begin{aligned} \mathbf{z}^T \mathbf{C} \mathbf{z} &= \mathbf{z}^T (\mathbf{A} + \lambda \mathbf{B}) \mathbf{z} \\ &= \mathbf{z}^T \mathbf{A} \mathbf{z} + \lambda \mathbf{z}^T \mathbf{B} \mathbf{z}. \end{aligned}$$

Note that for nonzero  $\lambda$ , the above equation is zero only when both  $\mathbf{z}^T \mathbf{A} \mathbf{z}$  and  $\mathbf{z}^T \mathbf{B} \mathbf{z}$  are zero since each term represents nonnegative energy. Recall that  $\mathbf{z}^T \mathbf{B} \mathbf{z}$  is the discretized version of

$$\iint (z_{xx}^2 + 2z_{xy}^2 + z_{yy}^2) dx dy$$

which becomes zero only when  $z(x, y)$  is a linear function over  $\Omega$ . Hence,  $\mathbf{z}^T \mathbf{B} \mathbf{z}$  is zero only when  $(p, q)$  is constant over the whole domain  $\Omega$ . On the other hand, from (2.8) and (4.1), we know that the term  $\mathbf{z}^T \mathbf{A} \mathbf{z}$  is zero only when  $\sum_{i=1}^{M_i} \Phi_i z_i = 0$  or, equivalently,  $\alpha_k p_k + \beta_k q_k = 0$  for every triangular domain  $T_k$ .

Thus,  $\mathbf{z}^T \mathbf{C} \mathbf{z}$  is zero only when  $\alpha_k p + \beta_k q = 0$  for every triangular domain  $T_k$  with respect to some constant  $(p, q)$ . This implies all  $(\alpha_k, \beta_k)$ ,  $1 \leq k \leq M_i$  are orthogonal to a certain  $(p, q)$ . Now, consider the case where two coefficients  $(\alpha_1, \beta_1)$  and  $(\alpha_2, \beta_2)$  are not linearly dependent. For  $\mathbf{z}^T \mathbf{C} \mathbf{z}$  to be zero, we have to require  $(p, q) = (0, 0)$ . In addition, if one nodal point is assigned with value  $c$ , it follows that  $\mathbf{z} = (c, c, \dots, c)^T$ .  $\square$

As discussed earlier, since only relative nodal heights have to be determined, we can pick an arbitrary point in reference to satisfy the first condition. The second condition usually holds in practice when we perform the local linearization of the reflectance map based on reconstructed surface obtained from the previous iteration. Therefore, the unique minimum of (5.5) can be easily guaranteed. Note that the conditions in Theorem 3 are sufficient but not necessary. For example, in the initialization stage of the successive linearization scheme described in Section III, even though condition 2 in Theorem 3 does not satisfy, the unique minimum of (5.5) is still guaranteed by conditions of Theorem 1.

We incorporate the regularization into the basic SFS algorithm to obtain a modified SFS algorithm, which is the algorithm used in our experiments described in Section VI.

#### Algorithm II: The Modified SFS Algorithm with Regularization

##### Initialization ( $k = 0$ )

Set the reference gradient  $(p_{0,i}^0, q_{0,i}^0)$  at triangle  $T_i$  to be  $(0, 0)$ , and construct the coefficient matrix  $\mathbf{C}^0 = \mathbf{A}_g^0 + \lambda \mathbf{B}$  and the load vector  $\mathbf{b}^0$ . Solve  $\mathbf{C}^0 \mathbf{z}^0 = \mathbf{b}^0$  for nodal values  $\mathbf{z}^0$ .

##### Iterations ( $k = 1, 2, \dots$ )

Set the reference gradient  $(p_{0,i}^k, q_{0,i}^k)$  at triangle  $T_i$  to be the local gradient determined by nodal values  $\mathbf{z}^{k-1}$ , and construct the corresponding coefficient matrix  $\mathbf{C}^k = \mathbf{A}_g^k + \lambda \mathbf{B}$  and load vector  $\mathbf{b}^k$ . Solve  $\mathbf{C}^k \mathbf{z}^k = \mathbf{b}^k$  for nodal values  $\mathbf{z}^k$ .

If  $\|\mathbf{z}^k - \mathbf{z}^{k-1}\| < \epsilon$ , where  $\epsilon$  is a predefined small quantity, then  $\mathbf{z}^k$  is the desired solution. Otherwise, go to the next iteration.

## VI. EXPERIMENTAL RESULTS

Our algorithm has been tested on several synthetic and real images. We use the global linearization scheme with respect to  $(p, q) = (0, 0)$  at the first iteration and perform local linearizations successively at the following iterations. The reconstructed surface of the previous iteration serves as the initial estimate of the current iteration, and therefore, the number of multigrid V cycles required to reach a given error bound decreases as iteration proceeds. The resulting algorithm is very efficient computationally. Similar to [9], [26], and [15], we choose the smoothing factor  $\lambda$  to be a certain small value at the first iteration and reduce the value gradually to near zero at following iterations.

To illustrate the quality of results, we present the 3-D surface plot of the reconstructed surface as well as three shaded views produced with three illuminating directions: the same, orthogonal, and opposite tilt directions with respect to the original lighting direction as suggested by Horn [9], [31].

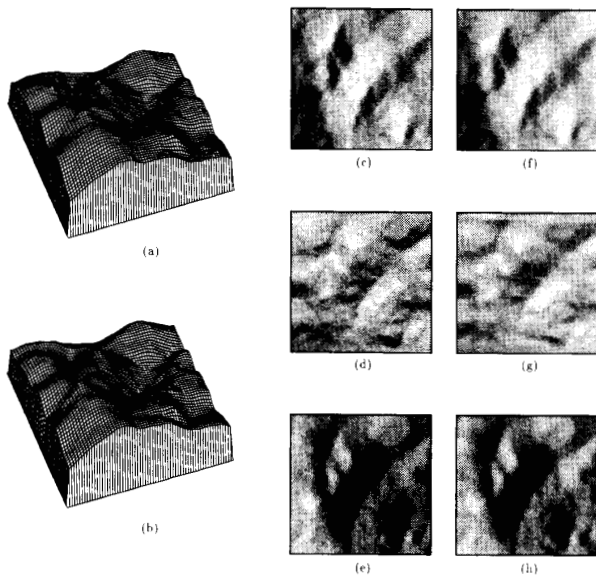


Fig. 5. Results of our algorithm applied to a synthetic  $64 \times 64$  DTM image: (a) Ground truth; (b) reconstructed surface; (c) image generated from ground truth with (tilt, slant, albedo, bias)=( $0^\circ$ ,  $50^\circ$ , 250, 0); (d) and (e) are shaded views of (a) with the opposite and orthogonal illumination direction, with tilt equal to  $90^\circ$  and  $180^\circ$ , respectively; (f)–(h) are shaded views of (b) with the lighting conditions used to generate (c)–(e), respectively.

**Test Problem 1: Terrain**

The tested image is a complicated synthetic  $64 \times 64$  image generated from the digital terrain model (DTM). Fig. 5(a) shows the original 3-D height plot, which is a wrinkled and steep surface (called the *alto-relievo* surface [9], [14]) of mountain area. The input image is generated by illuminating it from the east direction as shown in Fig. 5(c). The 3-D plot of the reconstructed surface is shown in Fig. 5(b). By comparing the true height in Fig. 5(a) and the reconstructed height in Fig. 5(b), they look very similar to each other. The shaded views of the reconstructed surface illuminated from the east, north, and west directions are given in Fig. 5(f)–(h). They should be compared with Figs. 5(c)–(e), which are generated by illuminating the true height from the east, north, and west directions, respectively. The corresponding shaded images appear to be almost the same.

The error of the reconstructed surface is plotted in Fig. 6(a), which is quite flat. To examine the error better, we present 1-D cross sections of heights in horizontal (parallel to the  $x$  axis) and vertical directions (parallel to the  $y$  axis) in Fig. 6(b) and (c), where the solid and dotted lines represent the original and reconstructed values, respectively. Note that the reconstructed surface is more accurate along the horizontal (east–west) direction in parallel with the illuminating source and less accurate along the vertical (north–south) direction. The same phenomena were observed for all our test problems and were reported in [9], [26]. Generally speaking, local fluctuations or ripples in parallel to the lighting direction occur in the reconstructed surface. They are particularly visible in the plane region.

It is worthwhile to point out that the phenomenon highly depends on the light source direction. Since different light sources result in different reflectance maps, it is possible to give an explanation by analyzing the property of reflectance maps. In [19], we perform a simple analysis of the reflectance map and show that the accuracy of reconstructed orientations or heights is closely related to the slope

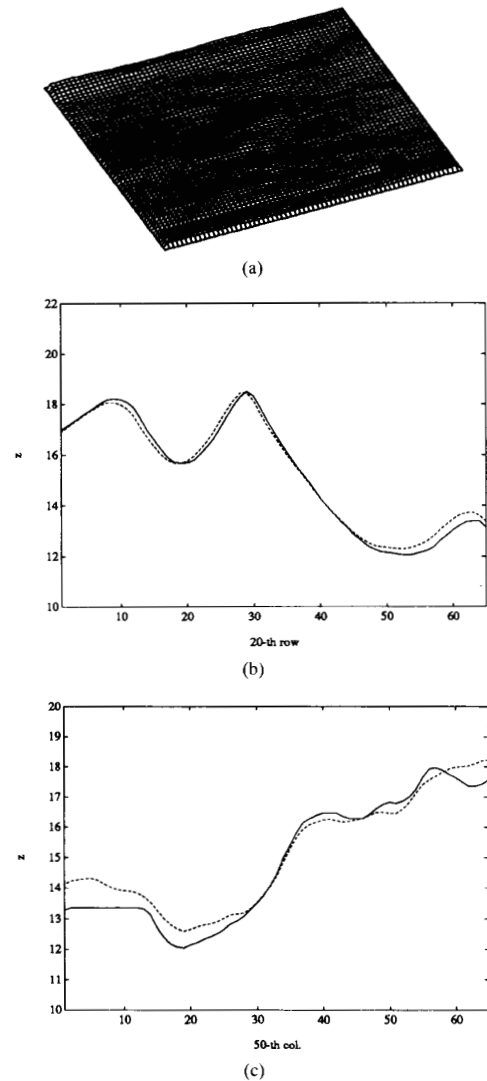


Fig. 6. (a) Three-dimensional plot of the height error; (b) 1-D cross section of original and reconstructed surfaces at 20th row; (c) 1-D cross section of original and reconstructed surfaces at 50th column.

of the reflectance map in the gradient space. This is an inherent limitation existing in the single-image SFS problem. Motivated by such an analysis, we propose a new scheme to overcome the limitation by combining multiple photometric stereo images with different reflectance maps [19].

**Test Problem 2: Lena**

The tested image is the  $256 \times 256$  Lena image as shown in Fig. 7(a). This image consists of both smooth and rapid varying areas with discontinuities in the surface orientation. The 3-D plot of the reconstructed surface and its shaded views illuminated with light sources from the same, opposite, and orthogonal tilt directions are shown in Fig. 7(b)–(c), respectively. This test problem is considered difficult since it contains several objects (possibly nonLambertian) with different reflectivities and shadows. Besides, the lighting condition is not ideal. However, with the assumption of homogeneous

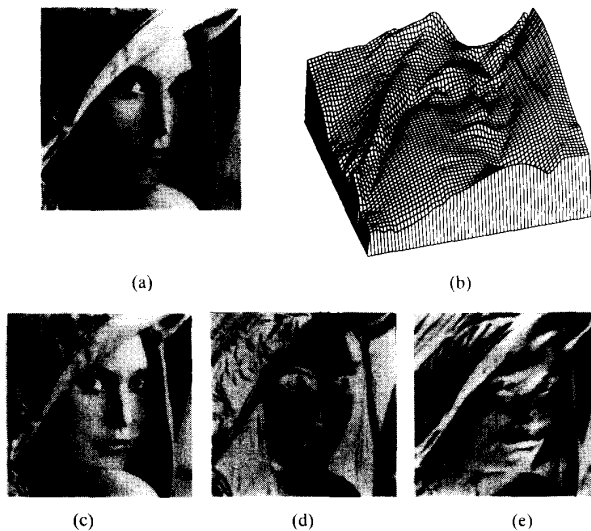


Fig. 7. Results of our algorithm applied to the  $256 \times 256$  Lena image: (a) Original image; (b) reconstructed surface with (tilt, slant, albedo, bias) =  $(30^\circ, 60^\circ, 25^\circ, 3)$ ; (c)–(e) are shaded views of (b) illuminated by the same, opposite, and orthogonal directions with tilt equal to 30, 210, and  $-60^\circ$ , respectively.

reflectivity and Lambertian over the entire image, our algorithm still produces good results. By comparing Fig. 7(c) with the original image in Fig. 7(a), we see that they are very similar. Pay special attention to the regions of face and shoulder. The shaded views illuminated from different directions in Fig. 7(d) and (e) also show that these reconstructed regions are satisfactory.

## VII. CONCLUSION

We presented a new efficient algorithm for the SFS problem in this research. Our algorithm recovers surface heights directly without any additional integrability constraint or artificial boundary assumption. It is based on a linear approximation of the reflectance map and a triangular element surface model, in which we express a surface as a linear combination of nodal basis functions. The nodal heights are determined by minimizing the cost functional, which is the total brightness error parameterized by nodal heights. This is equivalent to solving a large sparse linear system to which the efficient multigrid method can be easily applied. We discussed the existence and uniqueness of the solution by investigating the properties of the stiffness matrix. A regularization technique using the smooth surface constraint was introduced to ensure the well posedness of the SFS problem. A successive linearization scheme was developed to obtain increasingly correct surface and gradient information. Another advantage of our algorithm is that it maps naturally onto massively parallel architectures where each process covers one or several nodes.

## REFERENCES

- [1] M. Bertero, T. A. Poggio, and V. Torre, "Ill-posed problems in early vision," *Proc. IEEE*, vol. 76, no. 8, pp. 869–889, 1988.
- [2] M. J. Brooks, "Surface normals from closed paths," in *Proc. Int. Joint Conf. Artificial Intell.* (Tokyo, Japan), Aug. 1979, pp. 98–101.
- [3] R. Courant and D. Hilbert, *Method of Mathematical Physics*. New York: Wiley, 1962.
- [4] R. T. Frankot and R. Chellappa, "A method for enforcing integrability in shape from shading algorithm," *IEEE Trans. Patt. Anal. Machine Intell.*, vol. 10, no. 4, pp. 439–451, 1989; also in *Shape from Shading* (B.K.P. Horn and M. J. Brooks, Eds.). Cambridge, MA: MIT Press, 1989.
- [5] W. E. L. Grimson, *From Images to Surfaces*. Cambridge, MA: MIT Press, 1981.
- [6] B. K. P. Horn, "Shape from shading: A method for obtaining the shape of a smooth opaque object from one view," Ph.D. dissertation, Mass. Inst. Technol., Cambridge, MA, 1970.
- [7] ———, *Obtaining Shape from Shading Information*. Cambridge, MA: MIT Press, 1975.
- [8] ———, "Understanding image intensities," *Artificial Intell.*, vol. 8, no. 2, pp. 201–231, 1977.
- [9] ———, "Height and gradient from shading," *Int. J. Comput. Vision*, vol. 5, pp. 584–595, 1990.
- [10] B. K. P. Horn and M. J. Brooks, "The variational approach to shape from shading," *Comput. Vision Graphics Image Processing*, vol. 33, pp. 174–208, 1986; also in *Shape from Shading* (B. K. P. Horn and M. J. Brooks, Eds.). Cambridge, MA: MIT Press, 1989.
- [11] B. K. P. Horn and R. W. Sjöberg, "Calculating the reflectance map," *Applied Opt.*, vol. 18, pp. 1770–1779, 1979; also in *Shape from Shading* (B. K. P. Horn and M. J. Brooks Eds.). Cambridge, MA: MIT Press, 1989.
- [12] K. Ikeuchi and B. K. P. Horn, "Numerical shape from shading and occluding boundaries," *Artificial Intell.*, vol. 17, pp. 141–184, 1981; also in *Shape from Shading* (B. K. P. Horn and M. J. Brooks, Eds.). Cambridge, MA: MIT Press, 1989.
- [13] C. Johnson, *Numerical Solutions of Partial Differential Equations by the Finite Element Method*, Cambridge, UK: Cambridge University Press, 1987.
- [14] J. J. Koenderink and van Doorn, "Photometric invariants related to solid shape," *Optica Acta*, vol. 27, no. 7, pp. 981–996, 1980; also in *Shape from Shading* (B. K. P. Horn and M. J. Brooks, Eds.). Cambridge, MA: MIT Press, 1989.
- [15] Y. G. Leclerc and A. F. Bobick, "The direct computation of height from shading," in *Proc. IEEE Conf. Comput. Vision Patt. Recogn.* (Hawaii), May 1991, pp. 552–558.
- [16] C. H. Lee and A. Rosenfeld, "Improved methods of estimating shape from shading using light source coordinate system," *Artificial Intell.*, vol. 26, pp. 125–143, 1985; also in *Shape from Shading* (B. K. P. Horn and M. J. Brooks, Eds.). Cambridge, MA: MIT Press, 1989.
- [17] D. Lee, "A provably convergent algorithm for shape from shading," in *Shape from Shading* (B. Horn and M. Brooks, Eds.). Cambridge, MA: MIT Press, 1989, pp. 349–373.
- [18] K. M. Lee and C.-C. J. Kuo, "Shape from shading with a linear triangular element surface model," *Tech. Rep. 172*, Univ. Southern Calif., Signal Image Processing Inst., 1991.
- [19] ———, "Surface reconstruction from photometric stereo," *J. Opt. Soc. Amer. A.*, vol. 10, no. 5, pp. 855–868, 1993.
- [20] A. P. Pentland, "Local shading analysis," *IEEE Trans. Patt. Anal. Machine Intell.*, vol. PAMI-16, no. 2, pp. 170–187, 1984; also in *Shape from Shading* (B. K. P. Horn and M. J. Brooks, Eds.). Cambridge, MA: MIT Press, 1989.
- [21] ———, "Shape information from shading: A theory about human perception," in *Proc. Int. Conf. Comput. Vision*, 1988, pp. 404–413.
- [22] T. Poggio, V. Torre, and C. Koch, "Computational vision and regularization theory," *Nature*, vol. 317, pp. 314–319, 1985.
- [23] H. R. Schwartz, *Finite Element Methods*. New York: Academic, 1988.
- [24] G. B. Smith, "The relationship between image irradiance and surface orientation," in *Proc. IEEE Conf. Comput. Vision Patt. Recogn.* (Washington DC), June 1983, pp. 404–413.
- [25] T. Strat, "A numerical method for shape from shading for a single image," Master's thesis, Mass. Inst. Technol., Cambridge, MA, 1979.
- [26] R. Szeliski, "Fast shape from shading," *Comput. Vision Graphics Image Processing: Image Understanding*, vol. 53, no. 2, pp. 129–153, 1991.
- [27] D. Terzopoulos, "Multilevel computational processes for visual surface reconstruction," *Comput. Vision Graphics Image Processing*, vol. 24, pp. 52–96, 1983.
- [28] ———, "The computation of visual surface representation," *IEEE Trans. Patt. Anal. Machine Intell.*, vol. PAMI-10, no. 4, pp. 417–438, 1988.
- [29] A. N. Tikhonov and V. Y. Arsenin, *Method of Mathematical Physics*. Washington, DC: Winston and Wiley, 1977.
- [30] R. J. Woodham, "A cooperative algorithm for determining surface orientation from a single view," in *Proc. Int. Joint Conf. Artificial Intell.* (Cambridge, MA), Aug. 1977, pp. 635–641.
- [31] Q. Zheng and R. Chellappa, "Estimation of illumination direction, albedo, and shape from shading," *IEEE Trans. Patt. Anal. Machine Intell.*, vol. PAMI-13, no. 7, pp. 680–702, 1991.